International Journal of Applied Earth Observation and Geoinformation 139 (2025) 104495

Contents lists available at ScienceDirect

International Journal of Applied Earth Observation and Geoinformation

journal homepage: www.elsevier.com/locate/jag

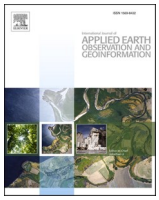

Automated crevasse mapping for Alpine glaciers: A multitask deep neural network approach

Celia A. Baumhoer [a,*], Sarah Leibrock [a,b], Caroline Zapf [c], Werner Beer [d], Claudia Kuenzer [a,b]

[a] German Remote Sensing Data Center (DFD), Earth Observation Center (EOC), German Aerospace Center (DLR), Weßling, Germany
[b] Chair of Remote Sensing, Institute of Geography and Geology, University Wuerzburg, Wuerzburg, Germany
[c] Nature Conservation & Cartography Division, German Alpine Club (DAV), Munich, Germany
[d] Digital Services Central Office, Austrian Alpine Club (ÖAV), Innsbruck, Austria

A B S T R A C T

Glacier crevasses are fractures in ice that form as a result of tension. Information on the location of crevasses is important for mountaineers and field researchers to plan a safe traverse over a glacier. Today, Alpine glaciers change faster than cartography can keep up with up-to-date manually created maps on crevasse zones. For the first time, this study presents an approach for automated crevasse mapping from high-resolution airborne remote sensing imagery based on a multitask deep neural network. The model was trained and evaluated over seven training and six test areas located in the Oetztal and Stubai Alps. By simultaneously preforming edge detection and segmentation tasks, the multitask model was able to robustly detect glacier crevasses of different shapes within different illumination conditions with a balanced accuracy of 86.2 %. Our approach is applicable to large-scale applications as demonstrated by creating high-resolution crevasse maps for the entire Oetztal and Stubai Alps for the years 2019/2020. Spatial and temporal transferability was proven by creating high-quality crevasse maps for all glaciers surrounding Großglockner, Piz Palü, and Ortler. The here presented datasets can be integrated into hiking maps and digital cartography tools to provide mountaineers and field researcher with up-to-date crevasse information but also inform modelers on the distribution of stress within a glacier.

1. Introduction

Crevasses are fractures in ice that form as a result of tension (Smith, 1976; van der Veen, 1998; Vaughan, 1993). Stress and strain develop due to vertical variations in ice velocity initiating starter microcracks at or near the surface of ice. These cracks propagate downward into the ice until reaching a point where the strength of the ice prevents them from penetrating further into the glacier (Nath and Vaughan, 2003). In the Alps, the depth of crevasses ranges from a few meters to 20–30 m with a width of 6–8 m as has been shown by field measurements. In contrast, the length of a crevasse can reach tens or even hundreds of meters (Ravanel et al., 2022). The sheer size of these crevasses poses a danger to mountaineers, rescue services and researchers at fieldwork especially when covered by snow bridges (Eder et al., 2008; Hohlrieder et al., 2010; Klocker et al., 2022; Taurisano et al., 2006). There are several strategies to avoid crevasse falls such as an early start and return time, walking in a rope team and optimal route planning. By walking in a rope team, crevasse falls remain without further consequences and are not recorded statistically. Despite these safety precautions, based on the 10-year average (2014–2023) annually 41 crevasse falls accidents happen in Switzerland and 13 in Austria that require mountain rescue services (Österreichisches Kuratorium für Alpine Sicherheit ÖKAS, 2024; Schweizer Alpen-Club SAC, 2024). In France, on average 13 crevasse falls require rescue services based on a 11-year average between 2008 and 2018 (Vanpoulle et al., 2021). Luckily, the mortality rate is low with two cases per year in Switzerland, one case per year in Austria (based on the 10-year average 2014–2023), and 3 cases in France (11-year average 2008–2018) (Vanpoulle, 2022). But in the face of climate change, crevasse falls will become more likely and traversing a glacier more difficult. In 2022, crevasse accidents (70 accidents) almost doubled compared to the previous 10-year average (38 accidents) because of glaciers with poor snow cover due to a winter with little snow and melting of the older snowpack uncovering previously filled crevasses (Schweizer Alpen-Club SAC, 2024, 2022). Therefore, it is more important than ever to provide maps with up-to-date crevasse zones for safe route planning.

In the Alps, information on crevasse zones is provided by classical cartography maps of the Alpine clubs in Austria and Germany, the Institut Géografique National in France, the Tabacco maps in Italy, and the Federal Office of Topography (swisstopo) in Switzerland. Today, glaciers change faster than cartography can keep up with time intensive manual mapping effort and field surveys. Therefore, information on crevasses in recent maps can be out dated and not sufficient to plan a safe traverse. The automated detection of surface crevasses from remote

* Corresponding author.
E-mail address: celia.baumhoer@dlr.de (C.A. Baumhoer).

https://doi.org/10.1016/j.jag.2025.104495
Received 7 September 2024; Received in revised form 5 December 2024; Accepted 19 March 2025
Available online 25 March 2025

sensing imagery can reduce the effort (Colgan et al., 2016) but is very challenging due to similarities with other surface features, requirements for high-resolution imagery and changing illumination conditions (Izeboud and Lhermitte, 2023; Shankar et al., 2023). Only few studies exist for ice sheets (Colgan et al., 2016; Izeboud and Lhermitte, 2023; Libert et al., 2022; Surawy-Stepney et al., 2023b), outlet glaciers (de Vries et al., 2023) and even fewer for mountain glaciers (Bhardwaj et al., 2016) requiring higher-resolution imagery. Traditional approaches used changes in the backscatter signal to identify crevasses in TerraSAR-X imagery (Marsh et al., 2021), brightness changes identified by different filters in ASTER imagery (Xu et al., 2011), Gabor filters for Sentinel-2 data (de Vries et al., 2023) or processing-intensive Sentinel-1 interferograms and a Canny edge detection algorithm (Libert et al., 2022). Newer developments apply neural networks for crevasse detection. Zhao et al (Zhao et al., 2022) applied a U-Net to map surface crevasses in Sentinel-1 SAR imagery (40 m spatial resolution) with an accuracy of 84.2 % (F1 score 72.5 %). Surawy-Stepney et al. (2023b) scaled-up crevasse mapping with a U-Net-like architectures and mapped crevasses from Sentinel-1 IW imagery (10 m spatial resolution) for entire Antarctica between 2015–2022 with a ROC accuracy between 91–93 % (depending on shelf). First experiments with foundation models such as the Segment Anything Model (SAM) (Kirillov et al., 2023) showed satisfying results for mapping glacial features (e.g. supraglacial lakes, icebergs, glacier termini) except for crevasse mapping were several manual feature definitions were necessary to produce segmentation results at all (44 % F1 score with prompts). Outside of the polar regions, ground penetrating radar (GPR) was used to detect crevasses in mountain regions (Eder et al., 2008; Zamora et al., 2007). Even though being a valuable tool for crevasse detection, GPR measurements require fieldwork and are only suitable for smaller local studies. The only study using remote sensing satellite imagery for glacier crevasse mapping was performed in the Himalayas for the Shaune Garang glacier. Crevasses were detected based on pan-sharpened thermal and short infrared Landsat imagery with a spatial resolution of 15 m and compared to GPS field measurements (root-mean-square error of 6.32 m for crevasse length, Bhardwaj et al., 2016).

To this day, no automated large-scale approach for Alpine crevasse mapping exists and existing approaches for ice sheets are not transferable to the Alps due to the insufficient spatial resolution and a different complexity of Alpine crevasses. The study by Marsh et al. (2021) detects crevasses by their backscatter signal in TerraSAR-X imagery. Even though the high-resolution spotlight imagery of TerraSAR-X (2 m, multilooked) would be sufficient to detect larger Alpine crevasses, the width of the crevasse does not correlate with the brightness profile. Meaning, that in areas with many small crevasses, signal overlays are likely and only rough locations of crevasses could be determined. The Gabor Crevasse Detector developed by de Vries et al. (2023) would be also applicable for high-resolution optical imagery but is unable to distinguish between linear features at the glacier surface. For Alpine glaciers this would impose the detection of all linear surface expressions including melt water channels, elongated debris on the glacier surface, healed crevasses and ascent paths. As these traditional approaches fall short in some aspects for Alpine crevasses, a number of studies explored convolutional neural networks (CNN) for crevasse detection. These approaches are predominantly based on a U-Net-like architectural design and demonstrated potential to automate crevasse detection over ice sheets (Lai et al., 2020; Surawy-Stepney et al., 2023b; Zhao et al., 2022). However, in the Alps these CNN-based methods are not yet applicable. The U-Net approach of Lai et al. (2020) was trained with 125 m resolution MODIS data being too coarse to detect Alpine crevasses. Zhao et al. (2022) and Surawy-Stepney et al. (2023b) detect crevasses with a U-Net architecture based on the backscatter signal in Sentinel-1 imagery at a resolution of 40 m and 50 m, respectively. Even when using higher resolution Sentinel-1 imagery at 10 m resolution, Alpine crevasses would be too narrow to create a strong backscatter signal which would allow the detection of individual crevasses by a U-Net. Furthermore, in general the segmentation approach with a U-Net tends to blurriness at the edges (Heidler et al., 2022). This effect might be minor for very wide crevasses and fractures present in Antarctica but substantial for Alpine crevasses only being several pixels wide and very close together. This problem can be solved by adding an edge detection task to semantic segmentation ensuring attention on clear boundaries as loss is monitored simultaneously for both tasks (Heidler et al., 2022). Using an edge detection approach alone would in contrast focus on edges in the imagery but would miss the semantic information on crevasse shapes learned by the semantic segmentation branch. Therefore, we want to take advantage of current developments in computer vision combining segmentation and edge detection and the availability of high-resolution remote sensing imagery to develop an automated crevasse detection algorithm for regular updates of hiking maps for safe routing and providing information on stress fields within a glacier for modelers. This objective rises the following research questions: (1) How can crevasses be mapped automatically from aerial imagery in the Alps? (2) How well performs a deep neural network for the automated mapping of glacier crevasses compared to common edge detection methods? (3) How transferable is this approach to other areas outside of the training regions? Our novel approach for crevasse mapping will provide accurate locations of crevasse zones and provide important information for safe Alpine tour planning with digital map services and provide glacier modelers with yet unprecedented information on stresses within a glacier.

2. Materials and methods

2.1. Study area

The study area covers the Oetztal and Stubai Alps with a glacier area of approx. 174.30 km^2 representing 53 % of Austria's glacier area (329.55 km^2) (BEV, 2024).The Oetztal Alps lost an area of 10.50 km^2 glaciated area between 1997 and 2006 (Abermann et al., 2009). The study area is located in an Alpine-dry region and climate change has impacted the regions infrastructure significantly. Especially the path network of hiking trails needs to be adapted on a regular basis and mountain huts are threatened by permafrost thaw. For example, glacier tongue retreat required the construction of a new suspension bridge over the Gurgler Ache gorge, where once a path led flat over the glacier tongue which cannot be crossed anymore without ice cover. The Hochwildehaus is closed since 2016 due to unstable ground resulting from permafrost thaw resulting in uncertain statics of the building. The Oetztal and Stubai are important tourism destinations with 5,2 million overnight stays in the tourism season 2023 (Land Tirol, 2024; Tourismusverband Stubai Tirol, 2024). Especially mountaineers are attracted by the Wildspitze (3768 m) being the highest peak of North Tyrol. Fig. 1 gives an overview of the study region showing the glaciated area in the Oetztal and Stubai Alps with examples of different crevasse types.

2.2. Datasets

In the Alps, glacier crevasse mapping requires high-resolution (<5 m) remote sensing imagery as their width ranges between sub-meter scale to a maximum of 6–8 m (Ravanel et al., 2022). This study uses open access orthophotos acquired in the years 2019, 2020 and 2022 by Land Tirol (data.tirol.gv.at) with a spatial resolution of 20 cm. For the Oetztal and Stubai Alps, a total of 1,076 orthophoto scenes were downloaded. These scenes were masked with glacier boundaries from the Austrian digital landscape model (BEV, 2024) which were manually optimized by the Austrian Alpine Club (ÖAV) to match the current glacier extent. After masking for glaciated areas, 446 scenes remained to create glacier crevasse maps.

Out of them, 15 scenes with varying crevasse and glacier morphologies present in the Oetztal and Stubai Alps were selected for training and testing the neural network. These 15 areas were defined manually

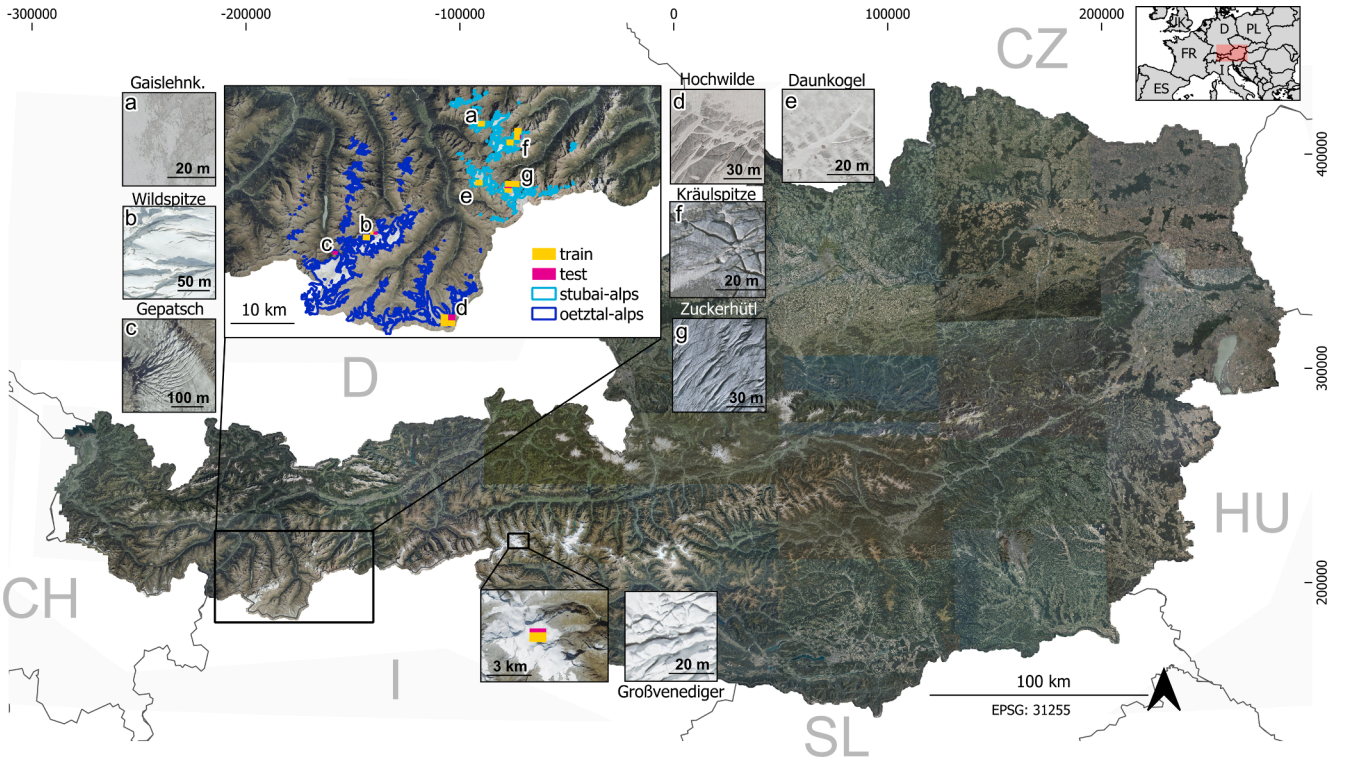

Fig. 1. Map of Austria showing the glaciated areas in the Oetztal (blue) and Stubai (turquoise) Alps. The enlarged image sections a-g show examples of different crevasse morphologies represented in the training and test dataset. The extent of the training and test region is visualized in orange and pink, respectively. Base map: *basemap.at*. (For interpretation of the references to colour in this figure legend, the reader is referred to the web version of this article.). (For interpretation of the references to colour in this figure legend, the reader is referred to the web version of this article.)

by browsing all available aerial imagery and selecting locations with the greatest possible variation in the appearance of crevasses that occur in Austria. Additionally, one scene over the Großvenediger was added to include large (>3 m width) crevasses covered by snow and icefalls (steep parts in the glacier with rapid flow resulting in a chaotic crevassed surface) not common in the Oetztal and Stubai Alps to this extent. Training and test regions are shown in Fig. 1 covering Wildspitze, Hochwilde, Western Daunkogel, Kräulspitze, Zuckerhüttl, Gaislehnkogel and Großvenediger. In total, an area of 16.13 km^2 is included in the training-validation dataset of which 6.92 km^2 account for glaciated area. The test dataset comprises six distinct scenes and encompasses 3.09 km^2, with a glacier area of 1.69 km^2. This results in an approximate train/test split of 80/20 as using 70 % or more of the dataset for training results in more accurate predictions (Bichri et al., 2024). During training, 10 % of the training dataset were reserved for validation ensuring to stop model training before overfitting. In the selection of training and test images, care was taken to cover all the different crevasse types in both the training and test datasets. The number of crevasse types varies greatly due to natural and regional differences in the occurrence of crevasse types. Transverse crevasses occur in 79 % of the imagery whereas splaying, longitudinal and marginal crevasses as well as bergschrunds (large crevasses at the top of glacier that separate moving ice from not moving ice above) occur only in less than 30 % of the imagery. Icefalls are least common and only represented in one scene in the Großvenediger area. For the significantly smaller test dataset marginal and transverse crevasses are most common, whereas splaying and longitudinal crevasses as well as bergschrunds and icefalls are only covered by one scene. Detailed information on the used orthophotos and a visual representation of the test and train dataset can be found in Table S1 and Fig. S2 in the supplementary materials.

2.3. Data preparation

Once the 15 scenes representing various crevasse types have been defined, the next step is to generate labels to provide the model with ground truth information during training. To minimize the manual effort, the Canny Edge detection algorithm implemented in the OpenCV Python package (Bradski, 2000) was used to create rough crevasse outline labels with manually adjusted thresholds per orthophoto scene. Afterwards, the labels were manually edited to add and remove outlines where the Canny Edge detection algorithm failed. The final manually edited ground truth labels include all visible crevasses and bergschrund locations. After rasterization of manually edited crevasse outlines, a one-pixel buffer (adding 20 cm on each side of the line) was applied to reduce the class imbalance of crevasse edge pixels compared to background pixels. Scenes included in the training dataset were tiled into 512 x 512 pixel tiles with a stride of 100 pixels including all three RGB channels. On each band, a percentile clip with a low threshold of 2 % and a high threshold of 98 % was applied for image enhancement and then normalized (min–max-normalization) globally in relation to the entire training dataset. All tiles with more than 20 % no data pixels were removed to speed up training time and enhance the number of tiles with high-information content. 8-fold augmentation (including the original image) was applied to increase our training dataset by all possible combinations of mirroring and rotation. This resulted in a total of 85,184 tiles for model training. The data preparation workflow is also shown in the flowchart describing the entire model training process in Fig. 2.

2.4. Crevasse mapping with HED-UNet

The HED-UNet is a multitask convolutional neural network (CNN) that was initially developed to detect calving fronts of Antarctic ice shelves from earth observation radar data (Heidler et al., 2022). The

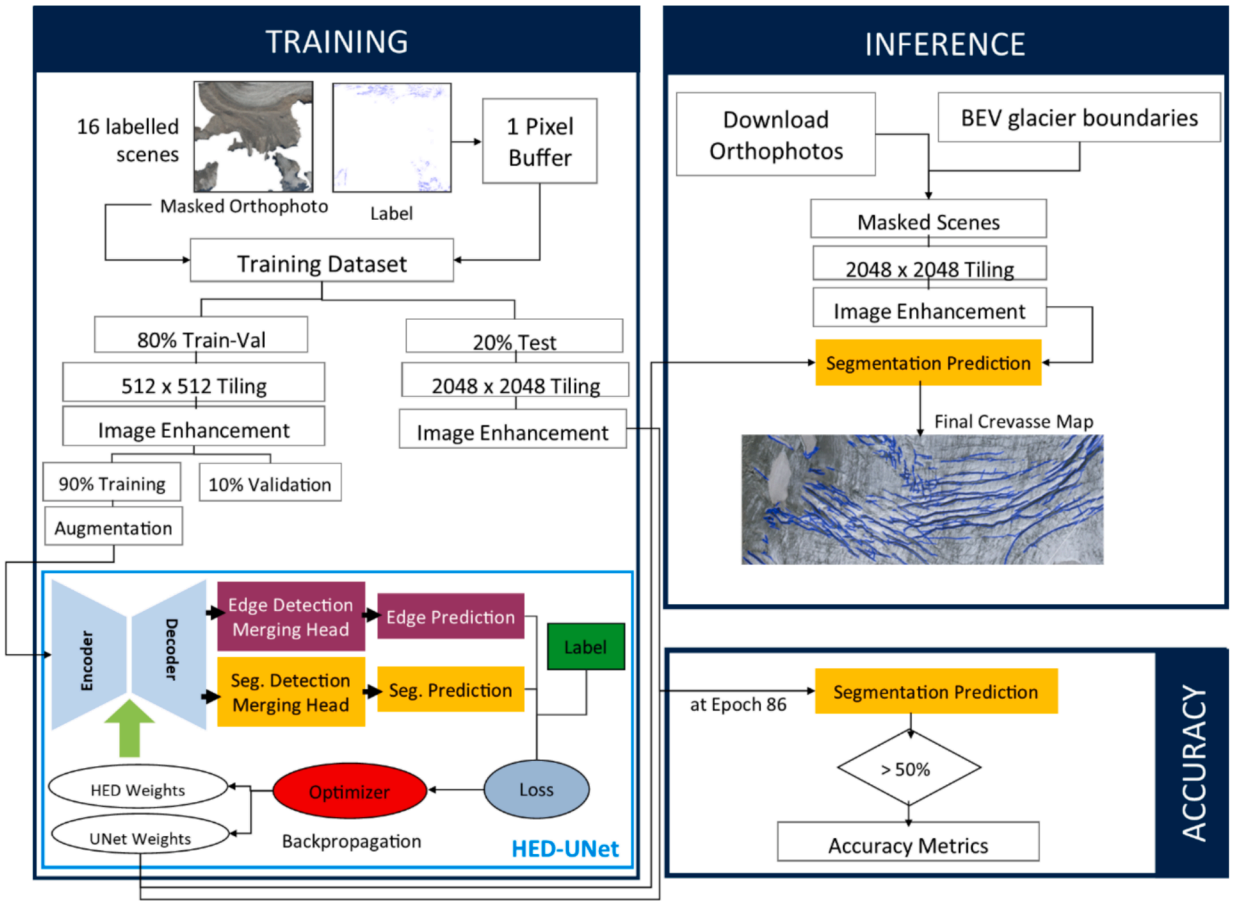

Fig. 2. Flowchart visualizing data preparation, model training, accuracy assessment and running the inference.

CNN combines edge detection and image segmentation in a multitask fashion by monitoring loss for both tasks simultaneously. The HED-UNet has an encoder-decoder architecture with six down- and upsampling blocks (see Fig. 2). The encoder calculates feature maps of different resolutions by downsampling to aggregate contextual information. This contextual information is re-distributed to the initial image resolution by upsampling in the decoder via skip connections. By creating deep feature pyramids, deep feature maps at lowest resolution might not be considered by the model. To avoid this, deep-supervision is implemented to create multiscale ground truth predictions. This enhances the receptive field of the model and encourages the network to better capture structures at all resolutions of the pyramid. Finally, the merging heads (one each for the segmentation and edge detection) combine the predictions at different pyramid levels into the final classification result for the edge detection and segmentation tasks separately. Merging is performed with hierarchical attention merging to attend to different resolution levels of all pyramid levels. This provides the model with large-scale information on glacier location and small-scale information for precise crevasse locations. The final output of the HED-UNet are two separate files with prediction probabilities for the edge detection task and for the segmentation task. For the here presented crevasse mapping approach we only use the output of the segmentation merging head as the edge predictions are at identical locations but wider. We adapted the HED-UNet to handle three channel RGB data instead of SAR data, optimized the image pre-processing for optical remote sensing data (percentile clip instead of decibel calculation) and decreased the initial tile size from 768 x 768 to 512 x 512 pixels to allow for larger batch sizes. All other parts of the model architecture are the same as in the original model by Heidler et al. (2022).

2.5. Model training

The HED-Unet was trained on a NVIDIA GeForce GTX 1080 Ti with 12 GB RAM for 100 epochs. Optimization of the model weights is done by Adam optimizer with the default learning rate of 0.001 (no grid search was performed to optimize for other learning rates than the default). We chose a batch size of 16 by empirically testing powers of two for the largest batch size fitting into the GPU's RAM and auto weighted binary cross entropy (AutoBCE) for training. AutoBCE is an adaptively balancing modification of the binary cross-entropy loss to equally weight both classes (crevasse, background) even though having a highly imbalanced dataset. Training for one epoch took 59 min. The best model was chosen by the epoch with the lowest validation loss at epoch 86 with a loss of 0.048 and an edge accuracy of 98.7 % for both, training and validation data. Inference (prediction of results) is performed on 2048 x 2048 pixel tiles and a stride of 265 to minimize computational cost and exploit all available GPU RAM. During inference, crevasse maps were created for the entire Oetztal and Sutbai Alps within 7.5 h where inference on one scene took one minute.

2.6. Accuracy assessment

The model was tested on 3.09 km^2 of data (1.69 km^2 glaciated) not used during training. The manual labels are considered as ground truth even though crevasse mapping is a very subjective task and results may vary strongly between cartographs. The test sites cover different crevasse morphologies to test the model performance for a maximum of variety including bare glacier ice, snow covered crevasses, ice falls, transverse, and splaying crevasses. Due to the lack of independent test data, we use manually tuned Canny Edge detection crevasse maps over

the test areas as a benchmark. We selected various classification accuracy metrics to assess the performance of our model as accuracy highly varies depending on how class imbalance is handled for calculation. Precision indicates how many pixels of the predicted crevasse pixels are in reality crevasse pixels and recall how many pixels are identified correctly of all ground truth crevasse pixels. Assessing both in conjunction is performed with the F1-score representing the harmonic mean of precision and recall. For these measures we used the macro-averaged and weighted recall, precision, and F1-score because of the high imbalance between crevassed and non-crevassed pixels. The macro-averaged approach is the unweighted mean of the metrics giving relatively high penalty for inaccuracies in the minority class of crevasses (Izeboud and Lhermitte, 2023). In contrast, the weighted version for precision, recall and F1-score accounts for the class imbalance. The specificity identifies how well true negatives are identified. To balance the model's performance on both classes, the balanced accuracy is a combined measure of macro-average recall and specificity to assess model performance based on balanced classes. Finally, the Cohen's Kappa quantifies the degree of agreement between two classifications beyond random coincidence (Cohen, 1960).

3. Results and Discussions

3.1. Glacier crevasse map for the Oetztal and Stubai Alps

Fig. 3 shows enlarged sections of the HED-Unet created crevasse map for the Oetztal and Stubai Alps. The example over Wazebachferner highlights the accurate detection of snow-covered crevasses (Fig. 3a). The outlines for crevasses on bare ice are shown for Eiskastenferner, Gepatschferner, Sulzenauferner, and Wilder-Freiger-Ferner (Fig. 3b,c,h, i). Examples of Marzellferner, and Wasserfallferner show the crevasse detection of snow filled crevasses on bare ice (Fig. 3e,f). Open bergschrunds were mapped at Hintereisferner and Sulzenauferner (Fig. 3d,g). Overall, one can observe that crevasses are outlined very accurately on bare glacier ice where crevasses are very prominent. Different shapes such as cross-cutting crevasses, icefalls, transverse crevasses or splaying crevasses are outlined clearly. The detection of snow-covered crevasses poses a greater challenge as only parts of the crevasses are detected at places where crevasses open up or snow bridges subsided compared to the surrounding area. Detecting the full width and length of these crevasses would require the use of longwave radar data or ground penetrating radar (Eder et al., 2008; Zamora et al., 2007) both not (yet) available for large-scale studies as presented here. Equally difficult is the mapping of snow-filled crevasses as longitudinal snow patches can remain on the glacier and may not necessarily represent a snow-filled crevasse. In these areas the model is very dependent on the manually labeled data it received during training. Hence, as presented in our manual labels, only snow-filled crevasses that are clearly recognizable are classified as crevasse. The detection of the bergschrund from optical imagery can be challenging due to the proximity to steep rock walls creating partial shadows on the bergschrund. The HED-UNet model was able to reliably detect open bergschrunds no matter of the illumination conditions. This shows the strength of deep convolutional neural networks in detecting properties based on their spatial context and morphology.

3.2. Glacier crevasse change in comparison to existing maps

Analysing glacier crevasse change is very challenging due to the limited availability of previous crevasse location information. The only available data source are maps created by cartographs of the German and Austrian Alpine Club over several decades. These maps are only available as image raster data whereby only a qualitative comparison on crevasse zones is possible. In Fig. 4 we compare crevasse zones from the DAV map for the Wildspitze (DAV, 2014) with our crevasse locations for four sample regions. For Sexegertenferner, Gepatschferner, and

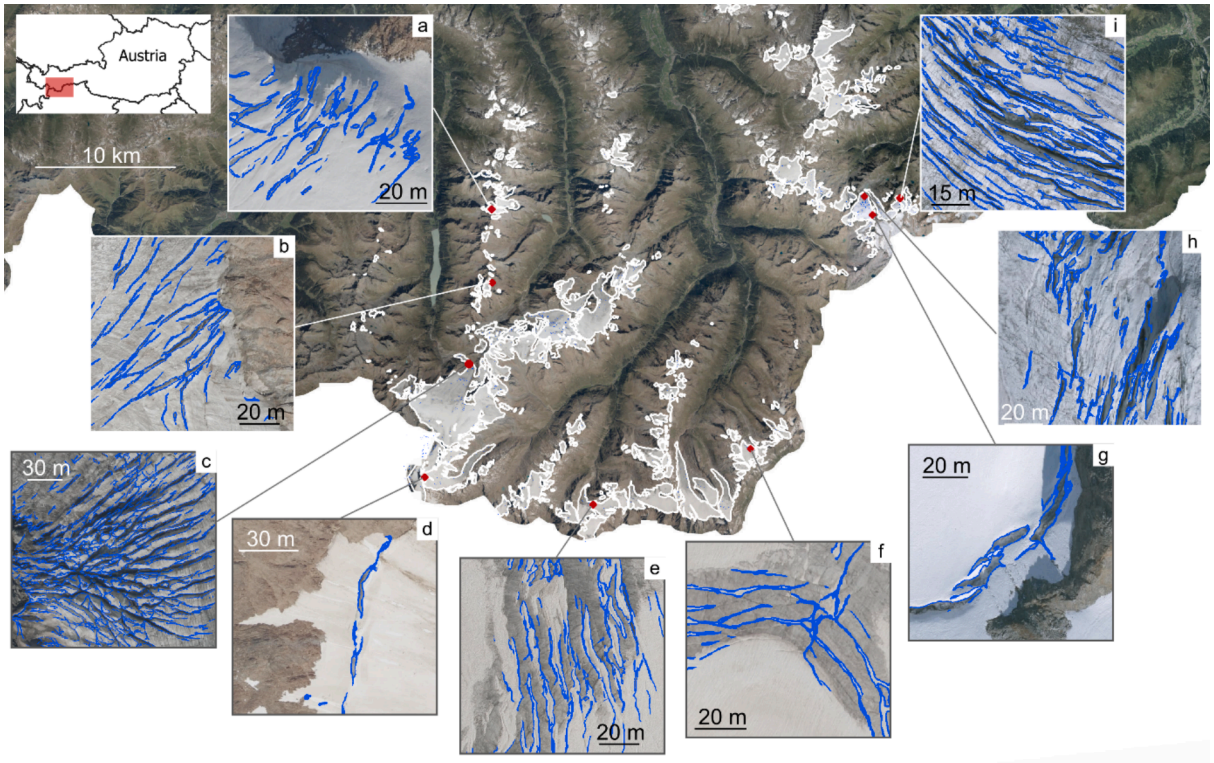

Fig. 3. Glacier crevasse map (blue) for the Oetztal and Stubai Alps with detailed examples for (a) Wazebachferner, (b) Mittlerer Eiskastenferner, (c) Gepatschferner, (d) Bergschrund of Hintereisferner, (e) Marzellferner, (f) Wasserfallferner, (g) Bergschrund and (h) crevasses at Sulzenauferner, and (i) Wilder-Freiger-Ferner. Base map: basemap.at. (For interpretation of the references to colour in this figure legend, the reader is referred to the web version of this article.). (For interpretation of the references to colour in this figure legend, the reader is referred to the web version of this article.)

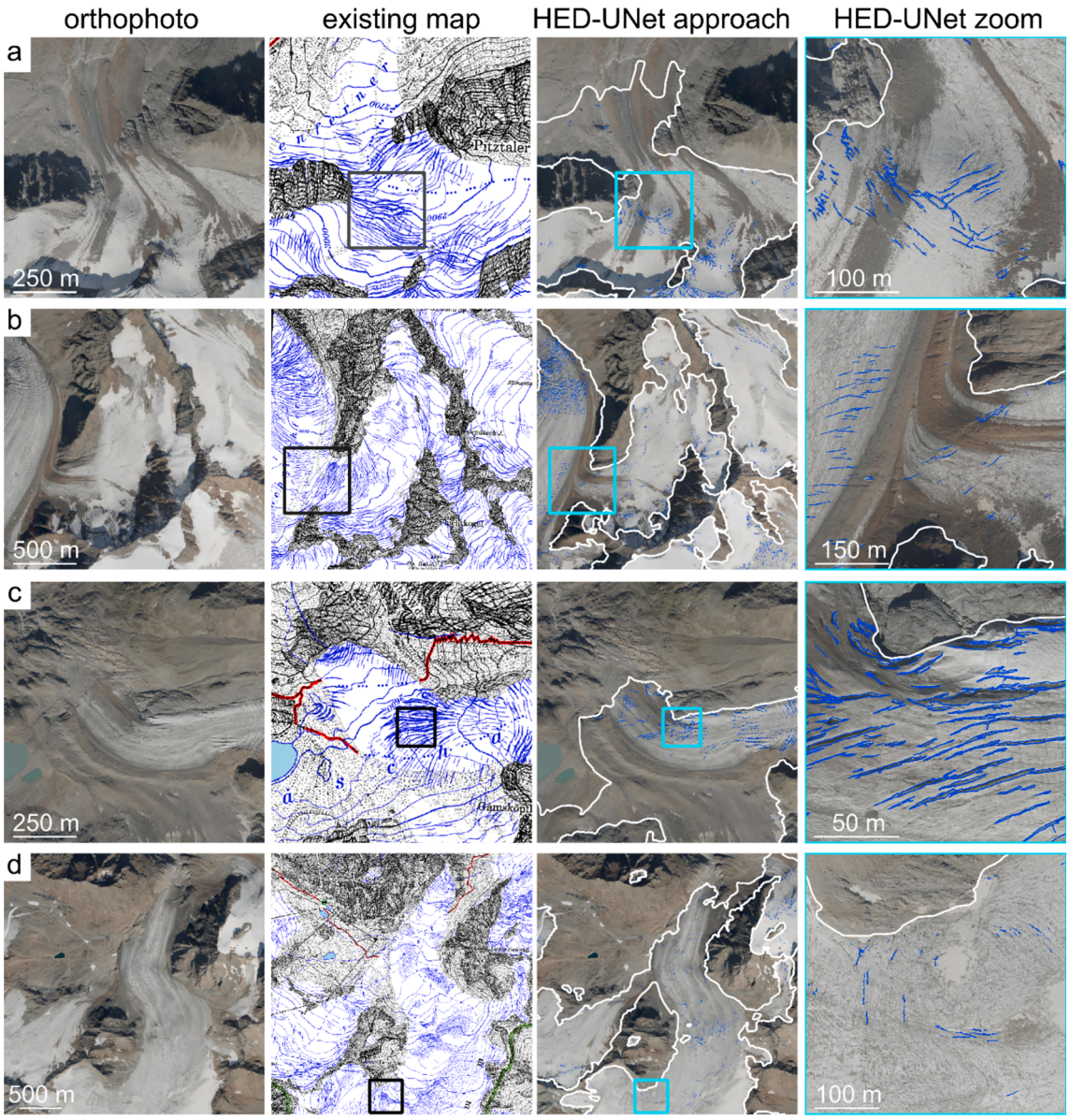

Fig. 4. Comparison of crevasse zones in existing map products and the results of this study for (a) Sexegertenferner, (b) Gepatschferner, (c) Taschachferner, and (d) Mittelbergferner with enlarged views (turquoise) of vanished or less prominent crevasse zones.

Table 1
Mean accuracy metrics for the test dataset compared to the Canny Edge benchmark and the results of HED-UNet.

		Canny Edge		HED-UNet	
		macro	weigh.	macro	weigh.
Precision (%)	$\frac{\text{True Positives (TP)}}{\text{Ture Positives (TP)} + \text{False Positives (FP)}}$	70.6	98.0	73.7	98.6
Recall (%)	$\frac{\text{True Positives (TP)}}{\text{Ture Positives (TP)} + \textit{FalseNegatives}(FN)}$	67.5	98.2	86.3	98.3
F1-Score (%)	$2\,\text{x}\frac{\textit{Recall}(R) \times \textit{Precision}(P)}{\text{Recall (R)} + \text{Precision (P)}}$	67.5	98.0	78.5	98.4
Accuracy (%)	$\frac{1}{n_{\text{samples}}}\sum_{i=0}^{n_{\text{samples}}-1} 1(\hat{y}_i = y_i)$	98.2		98.3	
Specificity (%)	$\frac{\text{True Negatives (TN)}}{\text{Ture Negatives (TN)} + \text{False Positives (FP)}}$	99.3		98.7	
Balanced Accuracy (%)	$\frac{\text{Recall (R)} + \textit{Specificity}(Sp)}{2}$	68.9		86.2	
Cohen's Kappa	$\frac{\text{Observed Agreement } (P_0) - \textit{ExpectedAgreement}(P_e)}{1 - \textit{ExpectedAgreement}(P_e)}$	0.38		0.57	

Mittelbergferner significantly fewer crevasses were detected. A closer look at the orthophotos confirms the absence from previously prominent mapped crevasse zones (Fig. 4a,b,c). The retreating glacier tongues of Taschachferner and Mittelbergferner have fewer crevasses at the front compared to the existing maps. Either the glacier is no longer present at the former mapped crevasse zone, or it has thinned to such an extent that only parts of the former crevasse zone remained (Fig. 4c,d). These examples highlight the importance for timely and regularly updated crevasse maps in the Alps due to recent rapid glacier change.

3.3. Accuracy of crevasse mapping results

Table 1 shows the results of the accuracy assessment for the Canny Edge detection benchmark and the HED-UNet generated results compared to the manual ground truth. For a visual interpretation, Fig. 5 shows different crevasse examples selected from the test data for the ground truth, Canny Edge detection, HED-UNet result and an overlaid, combined view. Overall, the HED-UNet approach outperforms the manually tuned Canny Edge detection result for every calculated metric except specificity explaining the true negative rate. This is related to the fact that the Canny Edge detection underestimates the extent of crevasses or does not recognize them at all hence false positives are very unlikely. Furthermore, the Canny Edge detection was used as a basis to create the manual labels and overlaps in correct regions for 100 %. In contrast, the HED-UNet sometimes extends crevasses beyond the manual label also missing out smaller crevasses in some cases as can be seen in Fig. 5c and 4e. Accuracies for recall, precision and F1-score are presented for calculations based on the macro-averaged and weighted

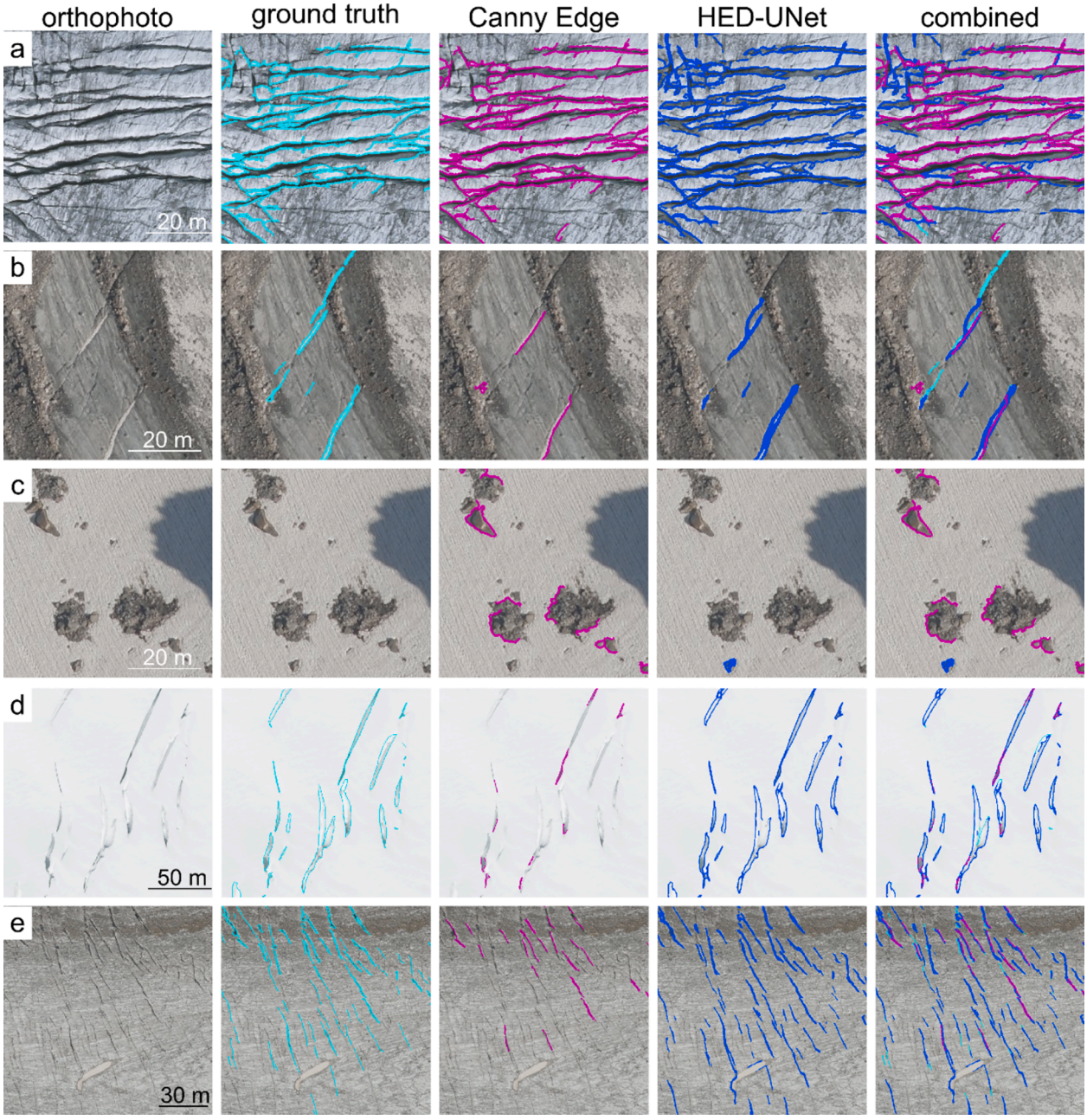

Fig. 5. Comparison between manually labeled ground truth (turquoise), Canny Edge detection (pink) and HED-Unet (blue) results on unseen test scenes located at (a) Sulzenauferner, Zuckerhütl (b,c) Langtaler Ferner, Hochwilde (d) Schaltenkees, Großvenediger, and (e) Taschachferner, Wildspitze. (For interpretation of the references to colour in this figure legend, the reader is referred to the web version of this article.). (For interpretation of the references to colour in this figure legend, the reader is referred to the web version of this article.)

approach.

The HED-UNet F1-score results for the weighted approach are higher than for the macro-averaged approach with 78.5 % and 98.4 %, respectively. This can be attributed to higher accuracies for the background class creating the majority of pixels and creating the class imbalance. When considering the macro-averaged approach (here false classifications for the crevasses are especially penalized) it is apparent that the precision is lower with 73.7 % compared to the recall with 86.3 %. In practice, this signifies that with a high recall, it is guaranteed that crevasses are mapped and not overlooked by our approach. This ensures that crevasse zones that present a risk to mountaineers are accurately mapped and enable the planning of safe routes. In contrast, the lower precision indicates the existence of false positive classifications, which can be attributed primarily to the misclassification of meltwater channels and debris on the glacier as crevasse. For mountaineers, this could result in the avoidance of direct routes and the planning of longer routes than necessary. The overall accuracy is high with 98.2 % for the Canny Edge detection and 98.3 % for the HED-UNet result. But as overall accuracy is misleading and inflating on imbalanced datasets, this accuracy measure should not be given too much attention and is rather listed for completeness. The balanced accuracy, considering class imbalance and also true negative classifications in contrast to the F1-score, is 68.0 % for Canny Edge detection and 86.2 % for the HED-UNet approach. The results demonstrate that the HED-UNet model is capable of accurately detecting crevasses, despite the presence of class imbalance and considering specificity. A high specificity demonstrates that the number of false positives (areas classified wrongly as crevasse) is very little and the classification of true negatives (glacier ice and surrounding correctly classified as no crevasse). This indicates that the mapped crevasse map only in very few cases leads to the planning of longer routes. Finally, the Cohen's Kappa results in a fair agreement for the Canny Edge detector with 0.38 and a moderate agreement for the HED-UNet approach with 0.57. Hereafter, the possibility of the agreement occurring by chance is high for the Canny Edge detector but lower for the HED-UNet approach. The statistical measures clearly demonstrate that the HED-UNet approach produces on average more accurate results. A comparison of the accuracies for the individual test scenes reveals significant discrepancies in performance, with the HED approach consistently demonstrating superior stability in balanced accuracy with 91–79 % compared to 89–58 % for the Canny Edge detector (see Table 2). Highest accuracies are achieved over bare ice with wide crevasses with both approaches as demonstrated for the region around Zuckerhütl at the Sulzenauferner (see Fig. 5a). The Canny Edge and ground truth labels are almost identical, as the ground truth was generated from the Canny Edge detections in areas of optimal performance. In addition, the HED-UNet identifies smaller linear features on bare ice as crevasse resulting in a slightly lower precision and over prediction. For the Langental Ferner at Hochwilde the accuracy is lowest for both approaches whereby the balanced accuracy for the HED-UNet (78.9 %) is significantly higher than for the Canny Edge (57.6 %) detector. This can be attributed to this specific test region where only few crevasses are present (see Fig. 5b) and only partly detected by the Canny Edge detector. Additionally, the test scene includes many small debris islands on snow where their boundary is always miss-classified by the Canny Edge approach but only in few cases by the HED-UNet (see Fig. 5c). When it comes to snow covered crevasses and icefalls the Canny Edge detector misses many crevasses due to the low image contrast. The considerably higher accuracy at Großvenediger with the HED-UNet (83.6 %) compared to the Canny Edge detector (60.3 %) underlines this as well as Fig. 5d. Superior performance is also achieved over bare ice with low contrast where the HED-UNet detects also smaller crevasses whereas the Canny Edge detector misses most of them (see Fig. 5e) on the Taschachferner close to the Wildspitze with a recall of 66.0 % versus 91.0 % for the HED-UNet.

Based on these accuracy metrics our approach produces comparable or even improved accuracies with existing studies. It should be mentioned here that these studies specialized in fracture and crevasse detection in the Antarctic and used different data sets (optical, SAR, lower spatial resolution) and accuracy metrics. Compared to the NeRD method, the HED-UNet produces comparable values for macro averaged precision and recall which is between 77 %-80 % for the NeRD method and 73 %-86 % for our approach. The macro averaged F1-score is comparable for the NeRD method (NeRD 80 % vs HED-UNet 79 %) and the accuracy of our approach is slightly higher with 98 % compared to 95 % for NeRD (Izeboud and Lhermitte, 2023). Surawy-Stepney et al. (2023a) only state the accuracies on the validation dataset in the training graph on the basic metrics such as recall, precision and F1-score (not macro averaged). These accuracies are outperformed by our approach for a recall of 81 % versus 98 %, precision of 78 % versus 99 % and an F1-score of 80 % versus 98 %, respectively. Zhao et al. (2022) test their approach on 10 visually interpreted SAR scenes producing slightly lower accuracies on average than this study with a precision of 81 % compared to 99 %, a recall of 73 % versus 98 % and an F1-score of 76 % compared to 98 %. The overall accuracy is also lower with 84 % compared to 98 % presented in this study (Zhao et al., 2022). These higher accuracies indicate the advantage of using edge detection simultaneously with segmentation than U-Net based segmentation alone. For sure, a more in-depth accuracy assessment based on a common benchmark dataset would be desirable to produce directly comparable measurements.

3.4. Limitations and challenges

Our novel developed crevasse detection approach outperforms existing approaches and can minimize manual mapping efforts

Table 2
Individual accuracy metrics for the Canny Edge benchmark and the HED-UNet results separately for each test scene with different crevasse types and snow conditions. High and low values are in bold.

No.	Test Scene	Area	Crevasse Type	Conditions
1	dop_2222_51_2019	Kräulspitze	transverse crevasses	bare ice, partly snow filled crevasses
2	dop_2221-42_2019	Zuckerhütl	longitudinal & marginal crevasses	bare ice, debris
3	dop_1920-32_2020	Wildspitze	transverse & marginal crevasses	bare ice, melt water channel
4	dop_3822-06_2022	Großvenediger	transverse crevasses & icefall	snow covered, low contrast
5	dop_2119-59_2020	Hochwilde	crossed crevasses	snow covered/filled, debris on snow
6	dop_1920-59_2020	Weißseespitze	marginal crevasses	bare ice, debris on bare ice

No.	Canny Edge (macro)					HED-Unet (macro)				
	F1	Precision	Recall	Bal. Acc.	Kappa	F1	Precision	Recall	Bal. Acc.	Kappa
1	62.5	61.1	64.5	64.5	25.0	78.3	73.4	85.9	85.9	56.6
2	**85.6**	82.8	89.0	**89.0**	**71.2**	**84.1**	79.9	89.8	89.8	**68.3**
3	70.8	80.0	66.0	66.0	41.6	80.8	74.8	91.0	**91.0**	61.7
4	64.4	76.3	60.3	60.3	29.3	78.4	75.3	82.6	82.6	56.8
5	**54.0**	52.7	57.6	**57.6**	**8.0**	**71.9**	67.6	78.9	**78.9**	**43.7**
6	77.3	78.7	76.1	76.1	54.7	77.4	71.2	89.3	89.3	54.9

significantly. For example, digitizing crevasses for one scene over Großvenediger took 24 h whereas the HED-UNet inference took one minute for the same area. Nevertheless, the high-resolution crevasse location information derived with the HED-Unet approach requires cartographic editing before it can be integrated into map products. The lower precision indicates the presents of false positive detections which could lead to unnecessary avoidance of specific areas. False positive detections can be observed over singular rocks on bare ice, man-made structures such as snow farms and ascent routes, elongated debris on snow, snow filled meltwater channels, and randklufts located in shaded areas (see Fig. 6). Even though, these false classifications exist, they only account for a small proportion. Especially, man-made structures such as snow farms and ascent paths as well as snow filled meltwater channels were not included in the training dataset as they are extremely rare in comparison to crevasses. Consequently, these features could not be learned during the training process. Whereas for modelers these false positive predictions may have little effects, for mountaineers and field researcher these can have large impacts especially when parts of a common ascent route are classified as crevasse. Hence, cartographic editing will still be required to provide trustworthy maps. But the crevasse mapping process itself is speeded up significantly with the crevasse dataset presented here.

To improve the automated crevasse detection over areas shown in Fig. 6 additional training data should be included focusing on training examples including ascent routes, snow farms and snow filled melt water channels. As these feature occur very rarely an option could be to create synthetically produced training data for such features (Hoeser and Kuenzer, 2022).

A limitation of mapping crevasses from optical remote sensing imagery is the ability to only map crevasses that are visible when snow-free during the ablation season, or very wide being visible despite snow cover. Even though we can accurately map visible crevasses very up-to-date there still remains the probability of missed crevasses covered with snow bridges year-round. Mapping hidden crevasses below snow would require ground penetrating radar surveys or airborne long-wave radar data penetrating deep into the snowpack. As these data are not available on a larger scale, we provide the best possible large-scale crevasse mapping product from optical data to this day. Furthermore, knowing that the majority of crevasse falls occur either in winter or in the summer months (July, August) (Klocker et al., 2022), the crevasse maps produced from the images taken in September should include the most dangerous crevasse zones for mountaineers. Especially, the more severe and deeper crevasse falls happening in winter can be avoided with the new crevasse maps presented here.

3.5. Spatial transferability of the crevasse mapping approach

To test the transferability of our approach, we have produced crevasse maps for the Großglockner region located at the border between Tirol and Kärnten, the Bernina Group in Switzerland, and the Ortler mountain in South Tyrol. This required slight modifications of the above described approach from Fig. 2. For Großglockner, the Austrian digital landscape model dataset (BEV, 2024) was used without manual edits and additional orthophotos were downloaded from the Land Kärnten with a different bit-depth. For Switzerland and Italy we used the glacier boundaries provided from the glacier inventory of the Alps for the years 2015/16 (Paul et al., 2020). We used aerial imagery with a spatial resolution of 10 cm of the year 2022 for the Bernina region (Swisstopo, 2022) and orthophotos with a resolution of 20 cm of the year 2023 for the Ortler (Autonome Provinz Bozen – Südtirol, 2023). We present the results of the inference run in Fig. 7 for Großglockner and in Fig. 8 for Piz Palü and Ortler. As no ground truth labels are available for these regions we only can provide a visual assessment of the transferability results. For Großglockner, crevasses of all different sizes and shapes are detected very accurately even if located in shaded areas or building circular shapes at the Pasterze which were not represented in the training data. In the Bernina Group crevasses are detected in most cases even over medial moraines. In the very steep icefall regions, some crevasse boundaries were missed due to high brightness and little contrast in the image. Additionally, the ascent route was wrongly detected due to the well-trodden path leading up to Piz Palü. Around Ortler, even crevasses covered by heavy debris were detected as well as

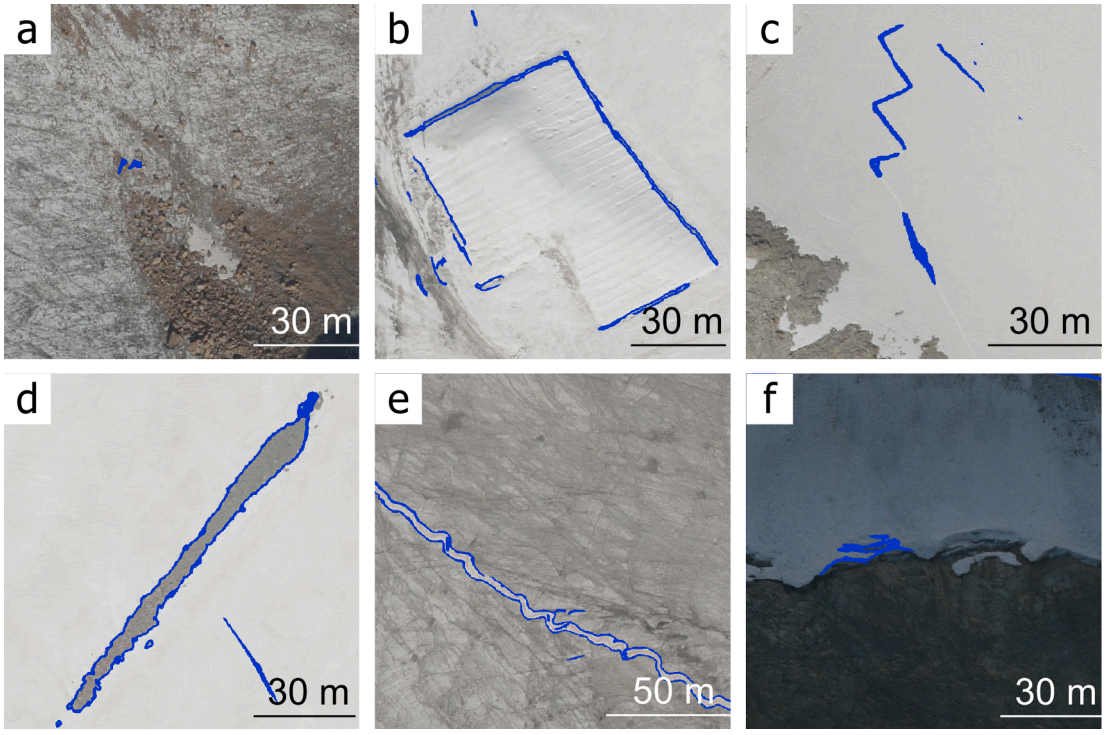

Fig. 6. False positive classifications can occur over (a) isolated rocks on the glacier, (b) man-made snow farms, (c) traces of an ascent route, (d) elongated accumulations of debris, (e) snow filled melt water channels, and (f) a randkluft in shaded area.

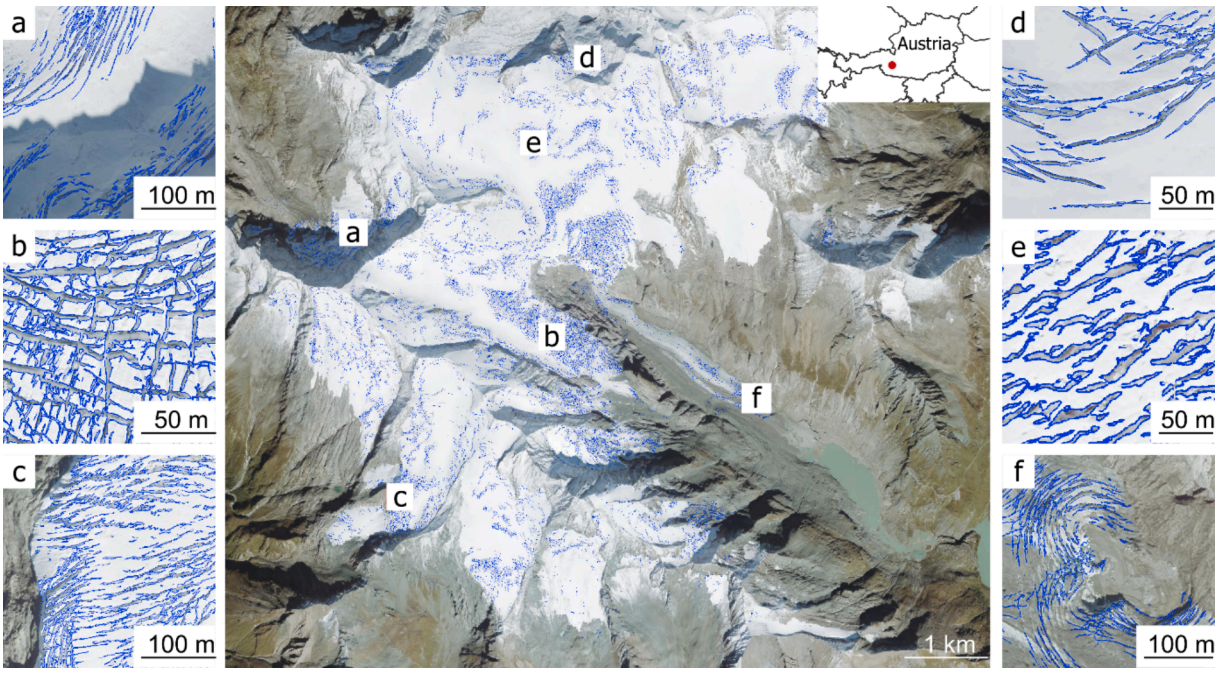

Fig. 7. Glacier crevasse map for the mountain range around Großglockner with Pasterze in the middle of the image (f). (a) Ödenwinkelkees, (b) Oberster Pasterzenboden, (c) Fruschnitzkees, (d) Karlingerkees, and (e) below Schattseitköpfl, Oberster Pasterzenboden. Base map: basemap.at.

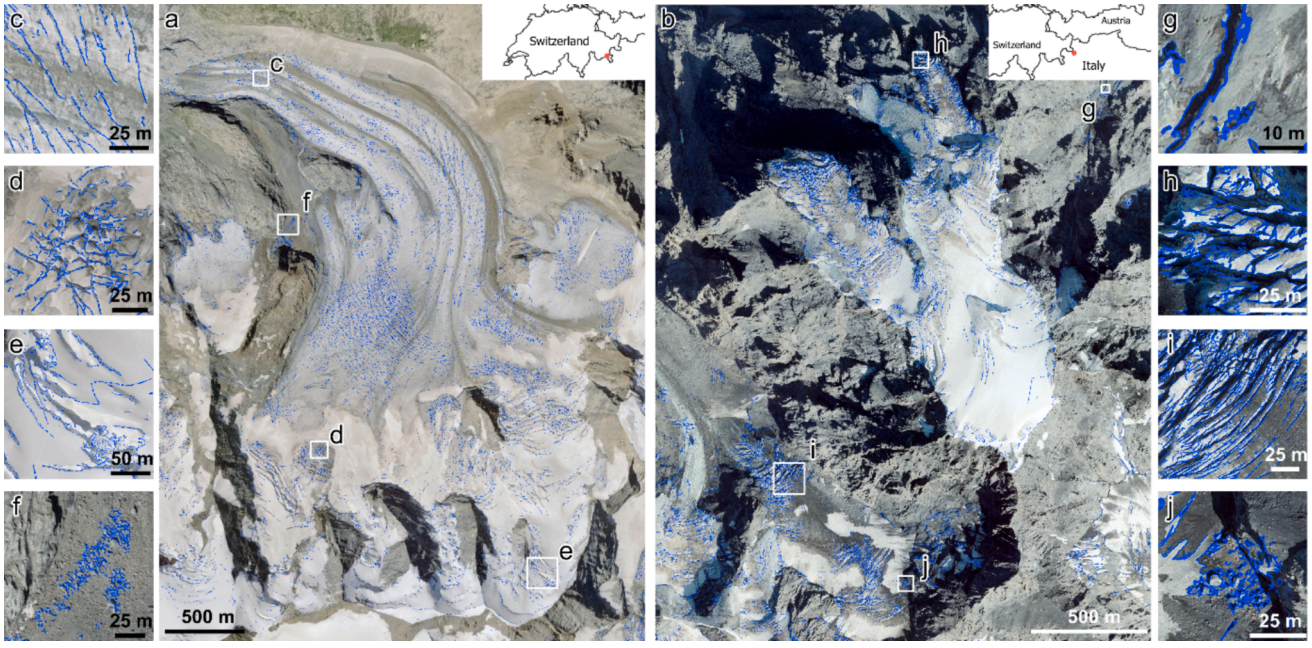

Fig. 8. Transferability test for the Pers Glacier below Piz Palü (a) and Ortler Ferner at the Ortler (b). Enlarged images around Piz Palü show crevasse detected at a medial moraine (c), crossed crevasses (d), icefall with ascent route (e), and wrongly classified debris due to the outdated glacier mask (f). For Ortler, enlarged views show debris covered crevasses (g), crevasses at a steep receding glacier tongue (h), crevasses within a debris covered glacier (i), and wrongly classified debris and snow patches due to outdated glacier mask.

crevasses at the steep and receding glacier tongues. For both regions, the not up-to-date glacier boundaries lead to false classifications in areas where the glacier retreated and only debris is left.

These results highlight the large-scale applicability of our approach and the potential for providing crevasse maps on country scale and beyond if high-resolution remote sensing imagery is available. For example, in Austria new orthophotos are acquired in regular time intervals and would allow updates every three to four years. In the face of climate change, it is crucial to ensure the use of up-to-date glacier boundary masks to prevent misclassifications in areas experiencing rapid glacier retreat.

3.6. *Future directions for crevasse mapping*

Automated crevasse mapping is just at the beginning, but it will undoubtedly evolve in tandem with advances in computer vision and deep learning-based image processing techniques but also the improved availability of high-resolution remote sensing imagery. Improved open

access availability of high-resolution imagery over mountain regions would enable large-scale crevasse mapping for other mountain ranges as well as multi-temporal analysis of crevasse formation. For sure, additional training imagery would be required for areas with a large amount of debris covered glaciers like the Himalayas. In addition, accurate and up to date glacier boundaries are required for the approach presented here. There are already good efforts to provide these on a global scale (RGI Consortium, 2023) but might not be timely enough for rapidly retreating glaciers due to climate change. False positive rates could be reduced by experimenting on advanced network designs such as cascading CNNs (Elharrouss et al., 2023), networks focusing on even more precise edge detections (Soria et al., 2023), and taking into account uncertainties in edge annotations (Zhou et al., 2023). It would be beneficial for future research to consider the possibility of detecting different crevasse types which can be beneficial for a better understanding of glacier dynamics (Li et al., 2024; Zhao et al., 2022). Including further data sources such as airborne LiDAR systems, laser altimeters (Li et al., 2024), ground penetrating radar (Walker and Ray, 2019) and holographic SAR tomography (Ponce et al., 2016) would be beneficial to estimate crevasse volume and to detect crevasses covered by snow bridges being invisible in optical remote sensing data.

4. Conclusions

For the first time, this study presents an automated crevasse mapping approach for mountain glaciers with potential for large-scale applications. Based on airborne optical remote sensing data, we trained a multitask deep learning neural network able to perform edge detection and segmentation tasks simultaneously. The model robustly detects glacier crevasses of different shapes within different illumination conditions. Large-scale applicability of our approach was demonstrated by creating high-resolution crevasse maps for the entire Oetztal and Stubai Alps. Applying our model for the Großglockner, Piz Palü and Ortler regions proves spatial transferability of the presented approach and potential large-scale applications for the future. The here presented datasets can be integrated into hiking maps and digital cartography tools to provide mountaineers and field researcher with up-to-date crevasse information. In addition to allowing safe routing on a glacier, crevasse maps indicate the distribution of stress within the ice mass and provide additional information for modelling internal ice dynamics and basal topography.

Data availability statement

The created crevasse maps for Oetztal, Stubai and Großglockner are freely available for download at https://geoservice.dlr.de/web/datasets/glacier_crevasses and registered at DOI Doi: 10.15489/fnjn62mbz324. The code for the HED-UNet is provided on GitHub (https://github.com/khdlr/HED-UNet) by Konrad Heidler. Aerial imagery is freely available by Land Tirol and Land Kärnten which can be downloaded at data.tirol.gv.at and kagis.ktn.gv.at. Glacier boundaries are available from the digital landscape model of Austrian land cover accessible at Doi: 10.48677/5db3e58e-3c6b-4bae-98e2-e57e706918da. Orthophotos of Switzerland can be accessed at https://www.swisstopo.admin.ch/de/orthobilder-swissimage-10-cm and at https://maps.civis.bz.it for South Tyrol. Alpine wide glacier boundaries can be accessed at Doi: 10.1594/PANGAEA.909133.

CRediT authorship contribution statement

Celia A. Baumhoer: Writing – original draft, Visualization, Validation, Software, Methodology, Data curation, Conceptualization. **Sarah Leibrock:** Writing – review & editing, Visualization, Software, Methodology, Data curation. **Caroline Zapf:** Writing – review & editing, Conceptualization. **Werner Beer:** Writing – review & editing, Data curation, Conceptualization. **Claudia Kuenzer:** Writing – review & editing, Supervision.

Declaration of competing interest

The authors declare that they have no known competing financial interests or personal relationships that could have appeared to influence the work reported in this paper.

Acknowledgements

The authors would like to thank Land Tirol, Land Kärnten, Swisstopo and the Province Bozen for providing high-resolution aerial imagery and Konrad Heidler for providing the HED-UNet architecture on GitHub.

Appendix A. Supplementary data

Supplementary data to this article can be found online at https://doi.org/10.1016/j.jag.2025.104495.

Data availability

The data supporting the findings of this study are openly available at DLR's GeoService: https://geoservice.dlr.de/web/datasets/glacier_crevasses; DOI https://doi.org/10.15489/fnjn62mbz324.

References

Abermann, J., Lambrecht, A., Fischer, A., Kuhn, M., 2009. Quantifying changes and trends in glacier area and volume in the Austrian Ötztal Alps (1969-1997-2006). The Cryosphere 3, 205–215. https://doi.org/10.5194/tc-3-205-2009.

Autonome Provinz Bozen - Südtirol, 2023. MapView - Landeskatographie [WWW Document]. URL https://mapview.civis.bz.it/ (accessed 10.24.24).

BEV, 2024. Digitales Landschaftsmodell - Bodenbedeckung Stichtag 07.05.2024 . Bundesamt für Eich- und Vermessungswesen. Doi: 10.48677/5db3e58e-3c6b-4bae-98e2-e57e706918da.

Bhardwaj, A., Sam, L., Singh, S., Kumar, R., 2016. Automated detection and temporal monitoring of crevasses using remote sensing and their implications for glacier dynamics. Ann. Glaciol. 57, 81–91. https://doi.org/10.3189/2016AoG71A496.

Bichri, H., Chergui, A., Hain, M., 2024. Investigating the Impact of Train / Test Split Ratio on the Performance of Pre-Trained Models with Custom Datasets. Int. J. Adv. Comput. Sci. Appl. 15. https://doi.org/10.14569/IJACSA.2024.0150235.

Bradski, G., 2000. The OpenCV Library. Dr Dobb's J. Softw. Tools Prof. 109 Program. 25, 120–123.

Cohen, J., 1960. A Coefficient of Agreement for Nominal Scales. Educ. Psychol. Meas. 20, 37–46. https://doi.org/10.1177/001316446002000104.

Colgan, W., Rajaram, H., Abdalati, W., McCutchan, C., Mottram, R., Moussavi, M.S., Grigsby, S., 2016. Glacier crevasses: Observations, models, and mass balance implications. Rev. Geophys. 54, 119–161. https://doi.org/10.1002/2015RG000504.

DAV, 2014. Alpenvereinskarte 30/6 Ötztaler Alpen Wildspitze. Deutscher Alpenverein, Munich.

Eder, K., Reidler, C., Mayer, C., Leopold, M., 2008. Crevasse detection in Alpine areas using ground penetrating radar as a component for a mountain guide system. Int. Arch. Photogramm. Remote Sens. Spat. Inf. Sci. 37, 837–841.

Elharrouss, O., Hmamouche, Y., Idrissi, A.K., El Khamlichi, B., El Fallah-Seghrouchni, A., 2023. Refined edge detection with cascaded and high-resolution convolutional network. Pattern Recognit. 138, 109361. https://doi.org/10.1016/j.patcog.2023.109361.

Heidler, K., Mou, L., Baumhoer, C., Dietz, A., Zhu, X.X., 2022. HED-UNet: Combined Segmentation and Edge Detection for Monitoring the Antarctic Coastline. IEEE Trans. Geosci. Remote Sens. 60, 1–14. https://doi.org/10.1109/TGRS.2021.3064606.

Hoeser, T., Kuenzer, C., 2022. SyntEO: Synthetic dataset generation for earth observation and deep learning – Demonstrated for offshore wind farm detection. ISPRS J. Photogramm. Remote Sens. 189, 163–184. https://doi.org/10.1016/j.isprsjprs.2022.04.029.

Hohlrieder, M., Kroesslhuber, F., Voelckel, W., Lutz, M., Mair, P., 2010. Experience with Helicopter Rescue Missions for Crevasse Accidents. High Alt. Med. Biol. 11, 375–379. https://doi.org/10.1089/ham.2010.1027.

Izeboud, M., Lhermitte, S., 2023. Damage detection on antarctic ice shelves using the normalised radon transform. Remote Sens. Environ. 284, 113359. https://doi.org/10.1016/j.rse.2022.113359.

Kirillov, A., Mintun, E., Ravi, N., Mao, H., Rolland, C., Gustafson, L., Xiao, T., Whitehead, S., Berg, A.C., Lo, W.-Y., Dollár, P., Girshick, R., 2023. Segment Anything.

Klocker, E., Meuli, L., Rauch, S., Kottmann, A., Mosimann, U., Pasquier, M., Métrailler, P., Doppman, P., Albrecht, R., Pietsch, U., 2022. Crevasse accidents in the Swiss Alps Epidemiology and mortality of 405 victims of crevasse accidents from 2010 to 2020. Injury 53, 183–189. https://doi.org/10.1016/j.injury.2021.08.010.

Lai, C.-Y., Kingslake, J., Wearing, M.G., Chen, P.-H.-C., Gentine, P., Li, H., Spergel, J.J., van Wessem, J.M., 2020. Vulnerability of Antarctica's ice shelves to meltwater-driven fracture. Nature 584, 574–578. https://doi.org/10.1038/s41586-020-2627-8.

Land Tirol, 2024. Tourismus in Tirol. URL https://www.tirol.gv.at/statistik-budget/statistik/tourismus/ (accessed 8.9.24).

Li, Q., An, J., Xing, Z., Wang, Z., Jiang, P., Yan, B., Wu, Y., Zhang, B., 2024. Three-dimensional dynamic monitoring of crevasses based on deep learning and surface elevation reconstruction methods. Int. J. Appl. Earth Obs. Geoinformation 132, 104017. https://doi.org/10.1016/j.jag.2024.104017.

Libert, L., Wuite, J., Nagler, T., 2022. Automatic delineation of cracks with Sentinel-1 interferometry for monitoring ice shelf damage and calving. The Cryosphere 16, 1523–1542. https://doi.org/10.5194/tc-16-1523-2022.

Marsh, O.J., Price, D., Courville, Z.R., Floricioiu, D., 2021. Crevasse and rift detection in Antarctica from TerraSAR-X satellite imagery. Cold Reg. Sci. Technol. 187, 103284. https://doi.org/10.1016/j.coldregions.2021.103284.

Nath, P.C., Vaughan, D.G., 2003. Subsurface crevasse formation in glaciers and ice sheets. J. Geophys. Res. Solid Earth 108. https://doi.org/10.1029/2001JB000453.

Österreichisches Kuratorium für Alpine Sicherheit ÖKAS, 2024. Alpinunfälle in Österreich 2023 - ein Jahresrückblick. URL https://alpinesicherheit.at/alpinunfaelle-2023-rueckblick/ (accessed 5.13.24).

Paul, F., Rastner, P., Azzoni, R.S., Diolaiuti, G., Fugazza, D., Le Bris, R., Nemec, J., Rabatel, A., Ramusovic, M., Schwaizer, G., Smiraglia, C., 2020. Glacier shrinkage in the Alps continues unabated as revealed by a new glacier inventory from Sentinel-2. Earth Syst. Sci. Data 12, 1805–1821. https://doi.org/10.5194/essd-12-1805-2020.

Ponce, O., Scheiber, R., Prats, P., Hajnsek, I., Reigber, A., 2016. Multi-dimensional airborne holographic SAR tomography reconstruction for glaciers at L-/P-band, in: 2016 IEEE International Geoscience and Remote Sensing Symposium (IGARSS). Presented at the 2016 IEEE International Geoscience and Remote Sensing Symposium (IGARSS), pp. 9–12. Doi: 10.1109/IGARSS.2016.7728993.

Ravanel, L., Lacroix, E., Le Meur, E., Batoux, P., Malet, E., 2022. Multiparameter monitoring of crevasses on an Alpine glacier to understand formation and evolution of snow bridges. Cold Reg. Sci. Technol. 203, 103643. https://doi.org/10.1016/j.coldregions.2022.103643.

RGI Consortium, 2023. Randolph Glacier Inventory - A Dataset of Global Glacier Outlines. Version 7. https://doi.org/10.5067/F6JMOVY5NAVZ.

Schweizer Alpen-Club SAC, 2024. Bergnotfallstatistik Die vergangenen Jahre in der Übersicht. URL https://www.sac-cas.ch/de/ausbildung-und-sicherheit/sicher-unterwegs/bergnotfallstatistik/ (accessed 5.13.24).

Schweizer Alpen-Club SAC, 2022. Vorsicht vor Spaltenstürzen auf Gletschern. URL https://www.sac-cas.ch/de/huetten-und-touren/achtung-vor-spaltenstuerzen-auf-gletschern-36256/ (accessed 5.13.24).

Shankar, S., Stearns, L.A., van der Veen, C.J., 2023. Semantic segmentation of glaciological features across multiple remote sensing platforms with the Segment Anything Model (SAM). J. Glaciol. 1–10. https://doi.org/10.1017/jog.2023.95.

Smith, R.A., 1976. The Application of Fracture Mechanics to the Problem of Crevasse Penetration. J. Glaciol. 17, 223–228. https://doi.org/10.3189/S0022143000013563.

Soria, X., Sappa, A., Humanante, P., Akbarinia, A., 2023. Dense extreme inception network for edge detection. Pattern Recognit. 139, 109461. https://doi.org/10.1016/j.patcog.2023.109461.

Surawy-Stepney, T., Hogg, A.E., Cornford, S.L., Davison, B.J., 2023a. Episodic dynamic change linked to damage on the Thwaites Glacier Ice Tongue. Nat. Geosci. 16, 37–43. https://doi.org/10.1038/s41561-022-01097-9.

Surawy-Stepney, T., Hogg, A.E., Cornford, S.L., Hogg, D.C., 2023b. Mapping Antarctic crevasses and their evolution with deep learning applied to satellite radar imagery. The Cryosphere 17, 4421–4445. https://doi.org/10.5194/tc-17-4421-2023.

Swisstopo, 2022. SWISSIMAGE 10 cm [WWW Document]. URL https://www.swisstopo.admin.ch/de/orthobilder-swissimage-10-cm (accessed 10.24.24).

Taurisano, A., Tronstad, S., Brandt, O., Kohler, J., 2006. On the use of ground penetrating radar for detecting and reducing crevasse-hazard in Dronning Maud Land. Antarctica. Cold Reg. Sci. Technol. 45, 166–177. https://doi.org/10.1016/j.coldregions.2006.03.005.

Tourismusverband Stubai Tirol, 2024. Kennzahlen Winter und Sommer. URL https://www.top.tirol/unternehmen/innsbruck-land/tourismusverband-stubai-tirol (accessed 8.9.24).

van der Veen, C.J., 1998. Fracture mechanics approach to penetration of surface crevasses on glaciers. Cold Reg. Sci. Technol. 27, 31–47. https://doi.org/10.1016/S0165-232X(97)00022-0.

Vanpoulle, M., 2022. Accidentologie des sports de montagne Combiner les approches quantitatives et qualitatives pour définir des axes de prévention. Lyon.

Vanpoulle, M., Lefevre, B., Soule, B., 2021. Mountaineering incidents in France: analysis of search and rescue interventions on a 10-year period (from 2008 to 2018). J. Mt. Sci. 18, 446–461. https://doi.org/10.1007/s11629-020-6208-y.

Vaughan, D.G., 1993. Relating the occurrence of crevasses to surface strain rates. J. Glaciol. 39, 255–266. https://doi.org/10.3189/S0022143000015926.

de Vries, M.V.W., Lea, J.M., Ashmore, D.W., 2023. Crevasse density, orientation and temporal variability at Narsap Sermia. Greenland. J. Glaciol. 69, 1125–1137. https://doi.org/10.1017/jog.2023.3.

Walker, B., Ray, L., 2019. Multi-Class Crevasse Detection Using Ground Penetrating Radar and Feature-Based Machine Learning, in: IGARSS 2019 - 2019 IEEE International Geoscience and Remote Sensing Symposium. Presented at the IGARSS 2019 - 2019 IEEE International Geoscience and Remote Sensing Symposium, pp. 3578–3581. Doi: 10.1109/IGARSS.2019.8899148.

Xu, T., Yang, W., Liu, Y., Zhou, C., Wang, Z., 2011. Crevasse Detection in Antarctica Using ASTER Images, in: Kamel, M., Campilho, A. (Eds.), Image Analysis and Recognition, Lecture Notes in Computer Science. Springer Berlin Heidelberg, Berlin, Heidelberg, pp. 370–379. Doi: 10.1007/978-3-642-21596-4_37.

Zamora, R., Casassa, G., Rivera, A., Ordenes, F., Neira, G., Araya, L., Mella, R., Bunster, C., 2007. Crevasse detection in glaciers of southern Chile and Antarctica by means of ground penetrating radar. IAHS Publ.-Ser. Proc. Rep. 318, 152–162.

Zhao, J., Liang, S., Li, X., Duan, Y., Liang, L., 2022. Detection of Surface Crevasses over Antarctic Ice Shelves Using SAR Imagery and Deep Learning Method. Remote Sens. 14, 487. https://doi.org/10.3390/rs14030487.

Zhou, C., Huang, Y., Pu, M., Guan, Q., Huang, L., Ling, H., 2023. The Treasure Beneath Multiple Annotations: An Uncertainty-Aware Edge Detector, in: 2023 IEEE/CVF Conference on Computer Vision and Pattern Recognition (CVPR). Presented at the 2023 IEEE/CVF Conference on Computer Vision and Pattern Recognition (CVPR), IEEE, Vancouver, BC, Canada, pp. 15507–15517. Doi: 10.1109/CVPR52729.2023.01488.